UNIVERSIDAD DE LAS PALMAS DE GRAN CANARIA
Facultad de Ciencias del Mar

# NEARSHORE CIRCULATION IN THE CONFITAL BAY

## Implications on marine debris transport and deposition at Las Canteras Beach

**Lydia Alicia Mcknight Morales**

Directed by: Dr. Germán Rodríguez Rodríguez

Dra. Marta Rodrigues

Dr. André B. Fortunato

A thesis submitted in partial fulfillment of the requirements for the degree of Master in Coastal Zone Management

**Máster Oficial en Gestión Costera**

2015/2016

# Table of contents

## List of figures

## List of tables

## Summary

This study attempts to expand knowledge on hydrodynamics in coastal regions and its impacts on debris transport and deposition. Hydrodynamics in the El Confital Bay (Gran Canaria, Canary Islands), a semi-enclosed basin including an urban beach in its inner part (Las Canteras Beach), with a high density of users and providing different recreational opportunities, is examined and related to marine debris collected at different locations along the beach. The whole bay constitutes a unique ecosystem with different habitats of national and international interest and the beach exhibits the particular geomorphological characteristic of being partially enclosed by a natural discontinuous rocky reef.

Experimental measurements of different hydrodynamic parameters are obtained for examining the circulation in the zone and to assess the performance of a circulation numerical model used to synthetize current fields under different metocean scenarios.

Information on marine debris collected on the shoreline during different beach surveys is examined and processed. Possible relationships between synthetic circulation patterns and debris occurrence and properties are explored.

## 1. Introduction

Oceans and coastlines are witnesses of the global pollution from marine debris during the last decades, and the social awareness of the impacts of this source of pollution is beginning to increase (Derraik 2002; Moore 2008; Yoon et al 2010; Vegter et al.,2014). Marine debris are defined as “any manufactured or processed solid waste material that enters the marine environment from any source” (Coe and Rogers, 1997) and are mainly composed by plastic items (Derraik, 2002; McDermid and McMullen, 2004). Because plastic products are lightweight, inexpensive and durable, they have become the most predominant materials for the consumers. However, these same characteristics make plastics a threat to ecosystems due to their persistence in terrestrial, aquatic, and marine environments (Barnes et al., 2009; Vegter et al., 2014).

The size of this type of pollutant covers a wide range, due to fragmentation process (Barnes et al., 2009), and because of this, it may produce many marine environmental impacts. Human communities are also affected directly and indirectly by this type of pollution, such as loss of tourism revenue and recreation value, increased cost of cleanups, threats to navigation and safety, contamination of food sources, loss of aesthetic value, and many others (Thompson et al., 2009; Yoon et al., 2010; Critchell et al., 2015; Blickley et al., 2016). Marine debris also affect the marine environment and human communities on the inhabited islands (Carson et al., 2013), such is the case of the first study in the Canary Archipelago, where even highly protected and inhabited areas were affected by marine debris (Baztan et al., 2014). Nevertheless, in general, the knowledge on this kind of pollution it is still very poor.

The sources of marine debris are extensive and can be ocean- or land-based (Coe and Rogers, 1997; Ryan et al., 2009). Land-based debris generally originate from urban and industrial waste

sites, sewage and storm-water outfalls, and terrestrial litter that reaches the waterways systems or even directly left by beach users (Ryan et al., 2009; Vegter et al., 2014). Population size, globally settled in coastal regions (Small and Nicholls, 2003), and the quality of the waste management systems determine the amount of land-based plastic debris entering in the ocean (Jambeck et al., 2015). Once the debris enters the marine environment, they can be transported elsewhere (Velander and Mocogni, 1998), or sink in the proximities (Somerville et al., 2003; Vegter et al., 2014). In contrast, ocean-based debris are materials either intentionally or accidentally dumped or lost overboard from vessels (e.g. Vegter et al., 2014).

Marine debris is mainly transported through a combination of wind and current patterns while tides, waves, and topographic local conditions, are the main responsible for coastal deposition and accumulation (Somerville et al., 2003; Carson et al., 2013; Baztan et al., 2014; Critchell et al., 2015; Liubartseva et al., 2016). However, some differences in main transport forces driving marine debris, in terms of its size, have been reported (Isobe et al., 2014). Hence, to improve the affection and management plans costs of this kind of pollution, such as benefits and the efficiency of beach clean ups as a mitigation tool, requires improving our understanding of transport mechanisms, as well as source and sink areas (Vegter et al., 2014). The development of field surveys (Rees and Pond, 1995; Velander and Mocogni, 1998), and the use of advantageous techniques such as numerical circulation models (Yoon et al., 2010; Liubartseva et al., 2016) are required to reach this objective.

Extensive environmental measures, such as protection of approximately half of the Archipelago's surface by international and national institutions (EUROPARC, 2014), are not sufficient to prevent plastic pollution from threatening the environment and affecting the main economic resource of the region.

In a large scale framework, due to its location, the archipelago is affected by the proximity of the North Atlantic Converge Zone (Maximenko et al., 2012). Marine debris tends to concentrate in these regions. Furthermore, the Canary Current may transport this pollution from the open Atlantic to the Canary Islands coasts, where it can be eventually deposited, such as suggested in the study performed by Baztan et al. (2014) in the more northeastern islands of the archipelago. However, transport and deposition of marine debris at specific sites strongly depends on local dynamical and geomorphological characteristics.

Nevertheless, no studies have been yet addressed this issue in Gran Canaria. In particular, due to Its location, geomorphological characteristics, and socioeconomic importance for the city of Las Palmas de Gran Canaria, Las Canteras Beach represents a natural landscape significantly vulnerable to the arrival of marine debris.

The present work aims to address, identify, and describe the characteristics and behavior of marine debris transport and deposition at Las Canteras Beach, by means of beach-based debris surveys and the study of meteorological and oceanographic dominant conditions, exploring the relationship between wind conditions and marine debris occurrence. For improving the understanding of the main circulation patterns, possible trajectories of materials on the surface waters, and its relationship between debris occurrence and different wind scenarios, a

circulation numerical model is applied. For future approaches, they can be used to identify high accumulation areas localization ("hot spots"), and contrast their relative importance in terms of their ecological role. Thus, it could be of great interest for establish baseline data for future actions and environmental management plans. This study does not attempt to predict the locations of accumulation for extreme conditions as, for example, during large storms or heavy rain episodes.

The rest of the study is structured as follows. Firstly, the second section describes the study area. Data acquisition methods and analysis are briefly explained in section three. Fundamentals of the numerical model are introduced in section four and experimental and numerical results are given in section five. Finally, main conclusions are exposed in section six.

## 2. Study area location and beach characterization

The Archipelago of the Canary Islands is located at the north-west African coast, nearly 100 kilometers west of the frontier between Sahara and Morocco. It is formed by seven main islands (from east to west): Lanzarote, Fuerteventura, Gran Canaria, Tenerife, La Gomera, La Palmas, and El Hierro. Due to their location, 29°15'N - 27°10'N and 19°00'W - 12°45'W, they are affected by sub-tropical climate, although this can vary with the location and topography. The islands are strongly affected by the prevailing northeastern winds, also known as trade winds, and by the Canary current heading south, which is a ramification of the southern flux of the Gulf's Current.

The beach of Las Canteras (Figure 1) is located at the northeastern coast of the Gran Canaria Island, and orientated towards the northwest (NW) within the Confital Bay, which is sheltered from the prevailing northeastern winds. Las Canteras is considered one of the few globally urban beaches visited throughout the year (Rodríguez et al., 2015). The beach is a 3 km long fine-grain blond sand beach, providing recreational opportunities to citizens of Las Palmas de Gran Canaria, the largest and most heavily populated city in the Canary Islands. The beach is bound to the north by a headland and southward by a groyne. It exhibits the particular geomorphological characteristic of being a semi-enclosed beach by a natural rocky reef of sedimentary origin, which runs parallel to the coast, separated approximately 200 m from the shore (Martínez et al., 1990). This morphological characteristic enables several different beach environments and uses. The southern end is exposed to the wave action, while the rest of the area is protected during low tide conditions. The beach is located within El Confital Bay (see Figure 1) which constitute a unique ecosystem with different habitats of national and international interest, declared as Special Conservation Zone (ZEC) and Site of Community Importance (LIC).


*Figure 1:Canary Islands Archipelago (top), Gran Canaria Island (bottom left), and Las Canteras beach with their sample transects locations (bottom right).*

Exposure to wave action changes along Las Canteras beach due to the discontinuities in its natural barrier. The aerial image of the study area reveals that the southern section of the beach is totally free from its protection. In the central area of the beach, known as “Peña La Vieja” the barrier is interrupted in two segments, allowing waves propagation through them, as well as the current flows pass through two deep channels formed. From this point to almost the end of northern part of the beach “La Puntilla” area is uninterrupted but another discontinuity is present at the very end of the beach. This features can be observed in Figure 1 (bottom right template) where the barrier can be easily detected by the presence or not of breaking waves. Note that in the southern part of the beach waves break on the beach due to the inexistence of barrier sheltering this zone against wave activity.

On the opposite side of the bay is located the Port Las Palmas, considered the main Port of the Archipelago and with numerous international connections (www.puertos.es) due to its strategic location at a crossroads between Europe, Africa and America. Consequently, it receives a large amount of shipping, cruise liner, and oil barge traffic. The results of this study cannot relate a direct affection of these activities, but can proportionate an illustrative approach of a possible debris source that could reach the area of interest. As a result, residents of the nearby areas are tied to the ocean, not only through a dependence on tourism and shipping, but also via aquatic activities that are integral part of their life style.

# 3. Data acquisition methods and analysis

Experimental information used in this study has been obtained from permanent measurements programs and through specific field surveys. Some data were also obtained from external sources whenever available. Due to the great variety of data required, this section will be divided into two main groups, marine debris and ocean-meteorological data.

## 3.1. Methodology for marine debris sampling

Due to the wide range of sizes (Barnes et al., 2009) and types found on marine debris throughout beach surveys, many different methodologies and type of materials to monitor have been reviewed (Hidalgo-Ruz et al., 2012). Nevertheless, it is obvious that the best methodology is one that adjusts to the main goal of study (e.g. Velander and Mocogni, 1999). Because the main object of the study is related within ocean-meteorological factors, it is interesting to capture only the recently debris transported by the sea, also known as "fresh debris" (Velander and Mocogni, 1999; Carson et al., 2013; Baztan et al., 2014), and not the items left behind by beach users or left from long time ago which would difficult even more its source identification. In addition, different management actions are occurring on the study area, such is the case of the cleaning services efforts, which could damage the samples if not taken into account. Nevertheless, if cleaning timetables and tools used are properly foreseen, its effects on field work can be minimized.

Samplings have to be also synchronized with tides intervals because it will determine the sampling allowance. Tide need to be low in order to allow the maximum debris collection due to intertidal surface exposure. To maximize the distance between the limits of the intertidal zone, low spring tides were chosen. Additionally, another day selection criterion needs to be taken into account. Sampling should not be carried out during weekends to avoid large quantities of debris left by users. Although cleaning services operate during late afternoons and night, exists the possibility that abnormal local debris amounts could not be totally recollected, so avoiding these days of higher densities of beach visitors is a safe bet.

It should be noticed that some studies (e.g. OSPAR, 2010) recommends to avoid, if possible, beaches nearby to urban areas for marine debris studies. Nevertheless, the advantage of the everyday cleaning, the easy site access for sampling, devices transport, and the all year round sand availability, makes Las Canteras Beach an adequate location for the study development.

To summarize, sampling periods were chosen to coincide with working days, spring tides, and when high tide falls inside the period between 23:00 hours and 02:00 hours. At this time no walking squad team works, until the next day at 06:00 hours, and when only the sand removal truck operates from 02:00 hours just on dry sand. This little available time space allowed debris collection on specific transects of Las Canteras Beach, and organization and speed was crucial for the sample success.

The sampling period covered more than one year, from November 2014 until March 2016, although only the last seven samples were finally considered due to adjustments on the

methodology used. The sampling interval was bi-monthly, and the selection of the sampling dates was carefully determined by taking into account the different factors above mentioned.

The sampling transects selection was done in order to represent the main different environments naturally present in the beach, time limitation for debris collections, and sand availability throughout the year. Sections of the beach where the high tide reaches all the way to the walk way, especially on spring time periods, where also avoided, because it could influence debris deposition (Baztan et al., 2014). Considering all the above, three transects were chosen for the monitoring period: La Puntilla (Tr1), Playa Chica (Tr2), and La Cicer (Tr3) Figure 1 (in yellow, blue and red circles respectively).

The Tr1-La Puntilla, northern end, represents a semi-closed environment and it is also the most sheltered place from the prevailing northeastern winds (Martínez et al., 1990). High sedimentary deposition occurs by light long-shore currents (Martínez et al., 1988). This transect is located on the proximity of a shelter area for small fisherman's boats. Transect Tr2-Playa Chica is also a semi-enclosed beach environment but with a steep shore and pocket beach morphology due to the course of the walkway. The last transect considered, Tr3- La Cicer, is on the southern limit of Las Canteras Beach and it is exposed to the wave action. The sedimentary environment on this transect differs from the others in seasonal sedimentary transport, grain size and composition terms (Martínez et al., 1990). For these reasons, the location of the transect was carefully chosen so it assured a sedimentary coverage throughout the year.

The monitoring plan carried on during the present study differentiates two types of sampling methodologies, which depends mainly on the size of the debris diameter. The size levels were established as a function of the cleaning squad capacity, which usually collect debris ranging from cigarette filters to bigger items, whereas smaller pieces are less likely left by beach users and not targeted by most cleanup efforts (Ryan et al., 2009). Because of these differences, and also to reduce time consumption during this process, the diameter thresholds between groups of debris was established as micro- (<5 mm), meso- (5-25 mm), and macro-debris (>25 mm).

#### 3.1.1. Meso- and micro- sampling and processing

After an extensive literature review, the sample methodology selected for this type of debris was a consequence of little time consumption during the sampling process and effective extraction of the desire materials sizes and types. Due to the environmental implications of smaller items of plastic in the environment and the aim of the study, only floating plastic materials were taken into account (e.g. McDermid and McMullen, 2004). The minimum limit size of collection established, >1 mm, was also determined by the main purpose of the present study. That is, to study the marine debris transport along the upper surface layers of the oceans by the effect of wind and currents. Buoyancy is affected by debris size (Isobe et al., 2004). Bigger floating objects tend to stay on the surface but no very small materials, affected by different process such as particle aggregation. Thus, considering items smaller than a couple of millimeters of diameter might be in conflict with the aims of the study. Although, some studies suggest that pellets, also known as virgin plastic pellets, are still influenced by the

effects of wind and surface currents (Ivar do Sul et al., 2009; Ivar do Sul et al., 2013). Because of the common size for pellets range from 1 to 5 mm (Hidalgo-Ruiz et al., 2012), the limit size established in this work seems to be quite reasonable.

Each sampling transect is 50 m length along the upper high tide water mark. The transect position was repeated for each sample date. The high tide line was selected because it holds much more plastic than other areas of the intertidal zone left by the receding tide (McDermid and McMullen, 2004; Hidalgo-Ruiz et al., 2012). This could be obvious because as we move seaward on the intertidal zone, wave induced dynamics is higher and little particles can be easily washed away and not stranded on the beach. Minimum width of the transect recommended on literature (Ryan et al., 2009) has been used, a total of six 0.25 $m^2$ (or 50 cm x 50 cm) quadrants of surface sediment evenly distributed 10 m apart, such as the depicted in Figure 2. The sediment was collected from a depth of no more than 1 cm, approximately, until a total of 1 L volume recipient was filled, and so, only the most recent tide deposited materials were collected.

Part of the sample processing was done in situ. The total of the six surface volume buckets was deposited in a 20 L tub previously filled with clean filtered seawater. The plastic fragments in the sample floated on the water surface, enabling to separate them from the rest of the sampled materials and remove them from the tub manually with a skimmer. This procedure was adapted from Hidalgo-Ruz et al. (2012) and has been also used in Baztan et al. (2014), but with different sediment volumes. The following procedure of the present work can be summarized as follows: density separation, filtration, sieving, and visual sorting of micro-plastics such as illustrated in Figure 3. The two first steps were done on field due to easily materials transport after density separation. The rest of the procedure was the most delicate and time consuming part due to count and classification process of very small particles through naked eye identification.

Before the sieving, samples were left drying under normal temperature conditions in a ventilated room, protected from the direct sunlight and abrupt changes of temperature, and any organic material was separated from the plastic. Through the sieving process, the particles were separated into four groups of size by passing them through a sieve cascade. The different particle size ranges used are:

- [>25]mm
- [>9-25]mm
- [>4-9]mm
- [>1.4-4]mm
- [<1.4]mm

For each size range, plastics were group into various categories (Figure 4): film, line, pellet, fragment or hard pieces, foam pieces (McDermid and McMullen, 2004), through carefully naked eye visual sorting and with help of magnifying glass for smaller pieces. Materials retained in the sieve were collected, while those that pass through were usually discharged or just taken into account the plastics pieces distinguishable by naked eye. To facilitate

identification of particles types, sign and marks of degradation and erosion on the surface caused by biological breakdown, photo-degradation, chemical weathering, or physical forces which could cause visible cracks, were considered (Hidalgo-Ruz et al., 2012). Materials corresponding to each size range and type group were counted and weighted on a balance accurate to 0.1 mg.

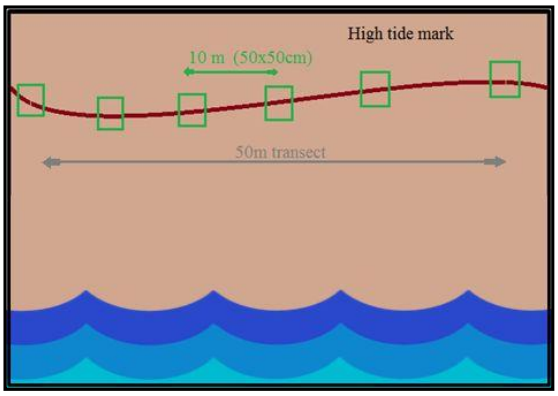


*Figure 2: Meso- and micro-debris sampling transect illustration.*

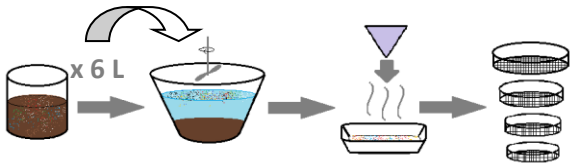


*Figure 3: Meso- and micro- debris sampling procedure.*

*Figure 4: Main meso- and micro-debris groups: Film (light blue), lines (orange), pellets (grey), fragments (yellow), and foams (dark blue).*

### 3.1.2. Macro-debris sampling and processing

The choice of the sampling and processing methodology for macro-debris (>25 mm of diameter) was also challenging due to the big amount of techniques and procedures used in previous studies. The procedure used in the present study was selected on the basis of the review and comparison of different methodologies by Velander and Mocogni (1999), which also recommended the selection of the one that best fits the goals of the study. Only “fresh debris”, or recently debris deposited by the last tide, was intended to be collected during low

tide conditions. Considering all the above, the method applied in the present study was the adaptation of the "Top bottom and vegetation lines" methodology. Higher strandlines tend to accumulate or present higher quantities of debris. Contrarily, the lower wet strandlines usually have only small amounts of litter, thereby spatial averages in these areas result in lower figures, but it is necessary to avoid overestimation of debris concentrations. Nevertheless, some modifications were made to the original sampling procedure adapt it to the main goals of the study. These modifications are related to transect length and sampling only upper and lower strandlines (or tide water marks), because vegetation line is only used when long-term accumulation debris is wanted. The original length established according to the bibliography 100 m, was not adequate due to time unavailability, lack of beach length and/or sedimentary materials along the transects (the case of Playa Chica or La Cicer transects). Consequently, a reduction to 50 m and 1 m of width, for both lower and upper strandlines, was done per transect (Figure 5). The covered area through this method was of 100 $m^2$. The transect positions were repeated for each sampling date and material belonging to this type was simultaneously collected with the meso- and micro-debris sampling, due to their upper strandline coincidence. Only debris items measuring greater than 25 mm were collected (approximately size of cigarette filters).

Before attempting to the classification and identification analysis, all collected debris was firstly rinsed off with water and left drying under normal temperature conditions, in a ventilated and direct sunlight protection room. Once debris was dried, all collected items were sorted and classified (Carson et al., 2013) according to the following general categories: plastic, rubber, processed lumber, clothing/fabric, paper/cardboard, and metal (Lippiat et al., 2013; Blickley et al., 2016) with some small modifications such as the union of plastic and rubber into "synthetic" main group (due to the entire synthetic rubber compositions collected), and the creation of a "Cigarettes filters" group. Cigarette butts were considered separately because of their predominant occurrence in comparison with the rests of the groups, which could hide variations in them. Main groups were further broken down originally into 36 subcategories, although after accomplishing the sample period and analyzing categories results, the subcategories were reduced into 21 categories (see Table 1) giving more attention to the synthetic subcategories. Each category item was counted and weighted on a balance accurate to 0.01 gr.

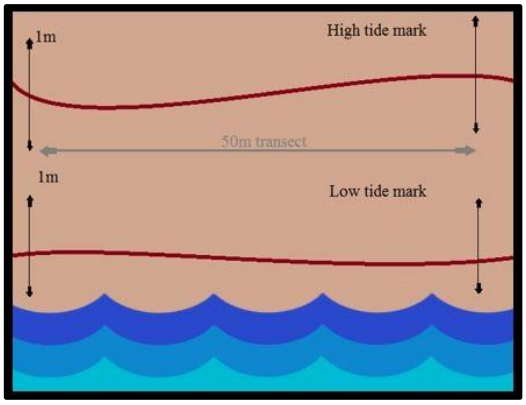


*Figure 5: Adaptation from Velander and Mocogni (1999), "Top and bottom line" methodology.*

*Table 1: Adapted from NOAA recommendations (2010). Classification table of marine debris items.*

| **Synthetic (A)** | | **Glass (B)** | **Code** |
|---|---|---|---|
| **Foamed** | **Code** | Glass fragments | B01 |
| Buoys and floats | A01 | **Cloth/fabric ( E)** | **Code** |
| Polystyrene fragments | A02 | Cloth and fabric | E01 |
| Packaging protection | A04 | **Processed lumber ( C)** | **Code** |
| Other polystyrene | A05 | Wood and lumber pieces | C01 |
| **Film** | A10 | **Aluminum/tinfoil (J)** | **Code** |
| **Hard plastic** | **Code** | Tinfoil paper or aluminum fragments | J01 |
| Plastic nets and ropes | A11 | **Other (G)** | **Code** |
| Beverage bottles | A12 | Unknown fragments | G01 |
| Food wrappers | A13 | **Paper/cardboard (D)** | **Code** |
| Bottle caps | A14 | Paper and cardboard pieces | D01 |
| Other hard plastic pieces | A15 | **Cigarettes filters (H)** | **Code** |
| Other jugs and containers | A17 | Cigarette filters /butts | H01 |
| Sanitary materials | A18 | | |
| **Rubber** | **Code** | | **Code** |
| Balloons | A21 | Other rubber fragments | A22 |

Another type of classification is through identification of possible source of materials through the main use or activity related of the materials before entering the waterways. This identification can only be applied on limited items, and results always should be taken with caution, which their unique type of usage could lead to a possible disposal source. Several studies suggest a large list of items whose source could be identify through this method, known as activities related debris (Velander and Mocogni, 1999; Ribic et al., 2012; Vegter et al., 2014; Blickley et al., 2016). Specific items such as plastic rope, monofilament line, nets, floats; as well as offshore activities common materials such as shipping containers or packaging bands (Ivar do Sul et al 2013; Vegter et al., 2014) could be directly related to fishing-related debris. Another specific group considered for source identification is that of medical or sanitary related waste, usually related with sewage debris or land –based debris, contains several uncertainties on its real disposal source. As a consequence, only marine-related debris have been considered in the present study. Only for illustration, the following table (Table 2) holds the list of the typical items found on related debris sources.

To identify items brought by the sea and without a clear marine-related activity relationship, was done through the identification of possible signs or marks on the material's surface (Figure 6Figure 6). The identification of origin source signs, such as high degradation, biofouling or bites marks (Somerville et al., 2003; Carson, 2013) on the surface could help us to assign the item a marine origin, or at least marine transport and not locally disposed, with a significant confidence. The rest of items with any of the cited signs detected, or possibly related to marine activities, were considered as unknown source because it could equally come from marine source (but stayed in the marine environment for a very short period of time) or locally disposed. Thanks to the cleaning efforts, and very little amount of beach users during the time of beach surveys, the locally disposal debris possibility can be considered low, but not null, and degradation signs method is appropriate because no item is left at the beach for a long period of time.

*Table 2: Possible list of items of marine-related debris source (blue), and other related-activities debris (grey).*

| Marine source | Medical /sanitary waste | Unknown source |
|---|---|---|
| **Nylon rope /net fragments** | Band aids | Beverage bottles |
| **Buoys/ floats** | Cotton butts | Plastic bags |
| **Fishing lures /line** | Sanitary napkin | Bottles and containers caps/ lids |
| **Light sticks** | Personal care products | Balloons |
| **Packaging bands** | syringes | Cigarette filters |

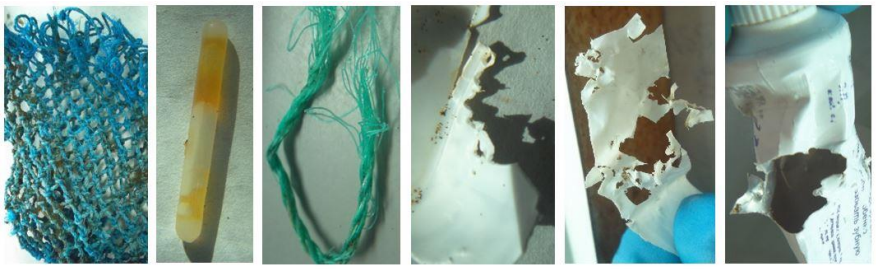

*Figure 6: Photographs of examples of fishing-related debris and bite marks.*

## 3.2. Ocean and meteorological acquisition data

### 3.2.1. Topography and bathymetry data

Topographic and bathymetric information are essential for establishing the numerical model and obtaining reliable results, which can be representative of reality observations. The topographic and bathymetric data used in the study is the result from the combination of different source of data, including LiDAR. The coastline was generated using LiDAR images obtained from GRAFCAN (2014), which covered the foreshore and dry area of Las Canteras Beach. The required bathymetric data for the model application were obtained from different sources. The large scale bathymetry was obtained from GEBCO (2014), which covered the entire archipelago (24.0897° and 34.0256° North latitude, and -21.9872° and -8.0769° West longitude, 30 arc-second spatial resolution). At the local scale, in the Confital Bay, the bathymetry used was obtained from the Ecocartographic project (Magrama, 2006). This last bathymetry has a resolution of 5x5 $m^2$ and include the beach of interest. All bathymetries were merged and linearly interpolated on top of each other from lower to higher resolution (Figure 7).

Due to the gaps between some of the bathymetries and the coastline morphology, a bathymetric filter and small modifications were made to improve the final bathymetry in the transition areas between bathymetries. All of the mentioned bathymetries where vertically referenced to Mean Sea Level (MSL). Due to the lack of enough detailed bathymetric information inside the barrier and beach domain, the grid was approximately defined with help of aerial photography, LiDAR data, and Confital Bay bathymetry values. Limitations of the bathymetry in the beach domain should be taken into account to assess possible mismatch between observations and models.

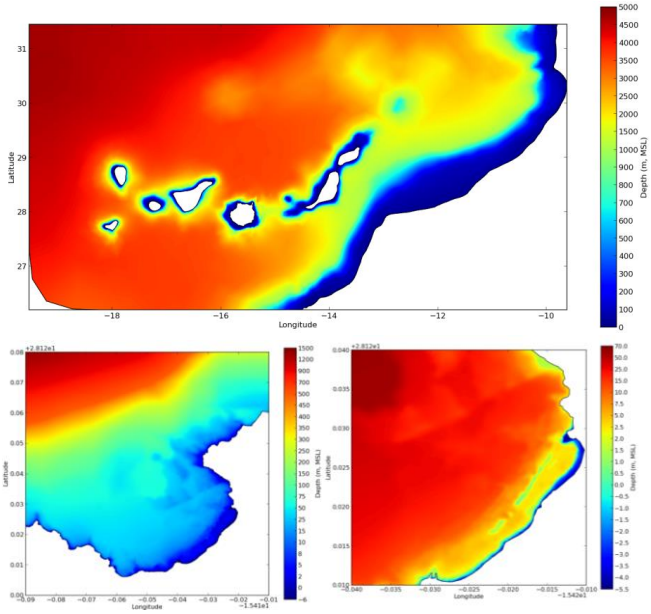

*Figure 7: Bathymetry of the study domain (top), Confital Bay (bottom left), and Las Canteras Beach (bottom right).*

### 3.2.2. Circulation data

Experimental current measurements have been recorded by using acoustic current meter deployed at a fixed position (Eulerian measurement) and GPS-drifters following the water track (Lagrangian measurements). Taking into account the study objective, main emphasis has put on data obtained by drifters following the trajectory of water parcels at the sea surface, while Eulerian measurements recorded at a given point at a "certain" depth below the surface have been used as additional information regarding to the model performance.

- *Lagrangians current measures*

Several GPS-drifters were released and tracked in the study area during different periods and under different meteorological and oceanographic conditions. Some of the trajectories followed by drifters are shown in Figure 8, where colors represent different measurements periods. Drifters tracking was supervised by from boats to avoid land or rock stranding. Right side of Figure 8Figure 8 shows photographs of a drifter from above and below sea surface.

- *Eulerian current measures*

Eulerian current measurements have been carried out by using an Aquadopp device, which uses the Doppler effect to measure current velocity in a small region inside the water column, which could be considered a single point current measurement. The instrument was deployed, during two days corresponding to equinoctial tidal conditions (September 29$^{th}$ to November 1$^{st}$ of 2015), with the sensors located 0.7 meters above the seafloor, approximately. The position of the current meter was chosen regarding its representativeness and total water column depth during low tides, but also bearing in mind additional factors, such as exposure to wind waves and presence of bathers. The location of the current meter as well as a photograph of the device installed are shown in Figure 9. Data recorded are the result of the average of values recorded during two minutes every twenty minutes.


*Figure 8: Lagrangian current measurements (left), drifters instruments (top and bottom right).*


*Figure 9: Aquadopp current meter location (green star) and photograph of the installed instrument.*

### 3.2.3. Sea level data

Sea level elevations data were obtained from the tide gauge of Las Palmas Port (www.puertos.es), located on the east side the Confital Bay. Hourly data recorded during 2014 and 2015 have been used. Due its proximity to the study area, tidal conditions at the measurement point are highly representative of that occurring at Las Canteras Beach, and was adequate for the purpose of verifying the predictions of the numerical model. The measures were transferred to MSL reference by the addition of 1.55 m established by REDMAR (Puertos del Estado, 2014).

### 3.2.4. Meteorological information

- *Wind data*

Wind data were obtained from a reanalysis study HIPOCAS spanning from 1958 to 2001 (Guedes Soares, 2008) (Figure 10), with a hourly time resolution, as well as from the wind estimated surface fluxes of the NCEP/NCAR reanalysis database (Kalnay et al., 1996) with a six hourly time resolution.


*Figure 10: Atmospherics reanalysis point located near to Confital Bay (www.puertos.es).*

# 4. Numerical circulation model

The application of numerical circulation models has numerous advantages for surface particle simulations and tracking, although the process can be challenging (Yoon et al 2010; Maximenko et al., 2012; Carson et al., 2013; Critchell et al., 2015; Liubartseva et al 2016). Due to the complexity of the processes to be simulated, the availability and quality of the input data, such as bathymetry or the atmospheric forcing, will determine the success and accuracy of the simulations.

The numerical current circulation model was applied during the trainee period at the National Laboratory for Civil Engineering (LNEC) of Lisbon, Portugal. The internship was part of the academic requirements, and its main goal was the implementation and exploitation in the study area of a numerical circulation model, SCHISM (Zhang et al., 2016), and of a particle-tracking model, VELApart (Oliveira and Fortunato, 2002). This application intended to understand the pathways of the waterborne materials on the surface waters, which will contribute to improve the knowledge and support the management of the marine waste found at the beach.

## 4.1. SCHISM model description

SCHISM (Semi-implicit Cross-scale Hydroscience Integrated System Model), is an open-source community-supported circulation model, which was developed from SELFE (Zhang and Baptista, 2008). Both models are designed for the effective continuous simulation of 3D baroclinic circulation along different scales (creeks, lakes, estuaries, open oceans). The improvements from the original model applied on SCHISM design included the addition of mixed triangle-quadrangles grid 1D/2D/3D options all wrapped in a single model. Mass conservation in SCHISM is enforced with the finite-volume transport algorithm and it naturally incorporates wetting and drying of tidal flats. SCHISM uses unstructured grids in the horizontal dimension, and hybrid SZ or the new LSC2 (Localized Sigma Coordinates with Shaved Cell) coordinates in the vertical. The main physical formulation of SCHISM is:

- Momentum equation: $\frac{\mathrm{D}\boldsymbol{u}}{\mathrm{D}t} = \frac{\partial}{\partial z}\left(v\frac{\partial \mathbf{u}}{\partial z}\right) - g\nabla n + \mathrm{F}$

- Continuity equation: $\frac{\partial \eta}{\partial t} + \nabla \cdot \int_{-h}^{\eta} \mathbf{u} dz = 0,$

$$\nabla \cdot \boldsymbol{u} + \frac{\partial w}{\partial z} = 0.$$

- Transport equation: $\frac{\partial C}{\partial t} + \nabla \cdot (\mathbf{u}C) + \frac{\partial wC}{\partial z} = \frac{\partial}{\partial z}\left(k \frac{\partial C}{\partial z}\right) + F_h + Q,$

Where:

$$\nabla\left(\frac{\partial}{\partial x}, \frac{\partial}{\partial y}\right).$$

$(x, y)$ horizontal Cartesian coordinates.

$z$ vertical coordinate, positive upward.

$t$ time

$\eta(x, y, t)$free surface elevation

$\mathbf{u}(x, y, z, t)$horizontal velocity, with Cartesian components $(u, v)$

$w$ vertical velocity

$\boldsymbol{F}$ other forcing terms in momentum (baroclinicity, horizontal viscosity,

Coriolis, earth tidal potential, atmospheric pressure, radiation stress.

$g$ acceleration of gravity, in [m s-2].

$C$ tracer concentration(e. g. , salinity, temperature).

$v$ vertical eddy viscosity, in $[\mathrm{m}^2 s^{-1}]$.

$k$ vertical eddy diffusivity in $[\mathrm{m}^2 s^{-1}]$.

$\boldsymbol{F}_h$horizontal diffusion

$Q$ mass source/sink

Further details about the model can be found in Zhang et al. (2015) and Zhang et al. (2016). The model implementation was developed following the steps illustrated in Figure 11.

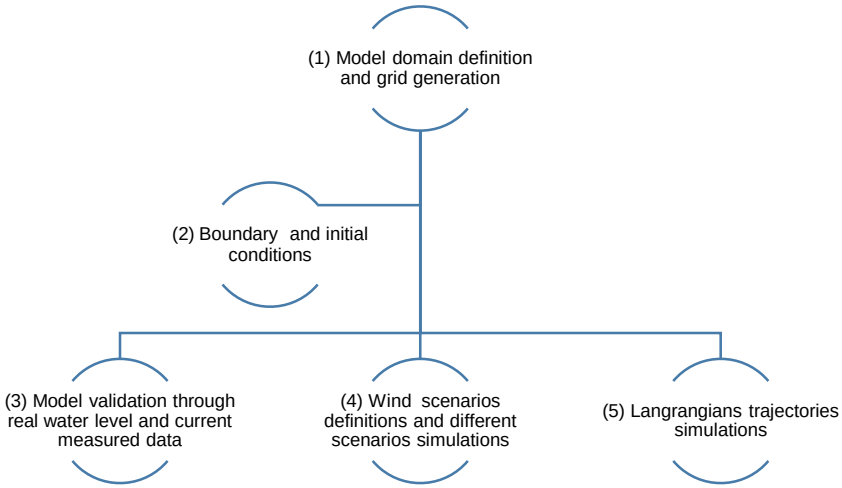


*Figure 11: Steps followed for the model implementation.*

## 4.2. Model domain definition and grid generation

The numerical model domain is defined by the surroundings of the Canary Islands Archipelago, so that all the different islands and possible interactions are represented. The coordinates of the grid are 26.195887° N and 31.448056° N and -19.52973° W and -9.6206543° W. This domain was represented on an unstructured triangular horizontal grid. The grid was refined in the area of interest and the bathymetry was added to the grid.

### 4.2.1. Grid

- *Horizontal grid*

The horizontal grid was elaborated with the XMGREDIT (Turner and Baptista, 1993), a tool that allows creating and editing finite element grids. The grid generated has a total of 50110 elements and 31082 nodes. The main steps followed for the grid generation were: extraction of a coarse grid from the grid of Fortunato et al. (2016), refinement of the elements near the study area, and interpolation of the different bathymetries into the final grid. The grid refinement was done by adding and decreasing the size of the elements in the area of interest. Firstly, a refinement was done around the island of Gran Canaria, and secondly, on the Confital Bay and Las Canteras Beach, until the adequate representation of the coastline was achieved. To improve the grid quality, NICEGRID tool was applied on the final grid, which improved the shape and positions of the elements that could cause problems on the model simulations.

After completing the grid, the land (closed) and water (open) boundaries were established. The resultant grid has a single open boundary with 67 nodes, relative to the external limit where the ocean continues, and 8 land boundaries with a total of 1005 nodes.

- *Vertical grid*

The definition of a vertical grid was needed to establish the 3D circulation model. A hybrid S-Z vertical grid was used, with 20 levels (11 Z levels and 9 equally S levels). The transition depth

between S and Z (hs) was located at 100 m. Three constants used in S-coordinate system of Song and Haidvogel's (1994), theta-b (θb), theta-f (θf) and surface/bottom thickness (hc), were also applied here. These constants control the discretization of the vertical levels along the column water. In the present work, a value of 1 was used on θb, which resulted in both bottom and surface being resolved, while a value of 5 at θf led to moderate skews along the water column but maintaining the surface and bottom resolution. A value of 30 was used in hc.

### 4.2.2. Bathymetry and topographic data addition

The addition of the bathymetry into the grid and the interpolation of the different bathymetries were major tasks, due to the variety of sources and formats of each bathymetry. Figure 12 represents the different domains and resolutions of the bathymetry in the entire domain, the island of interest and the beach. The noticeable refinement of the grid close to Las Canteras Beach is also shown.

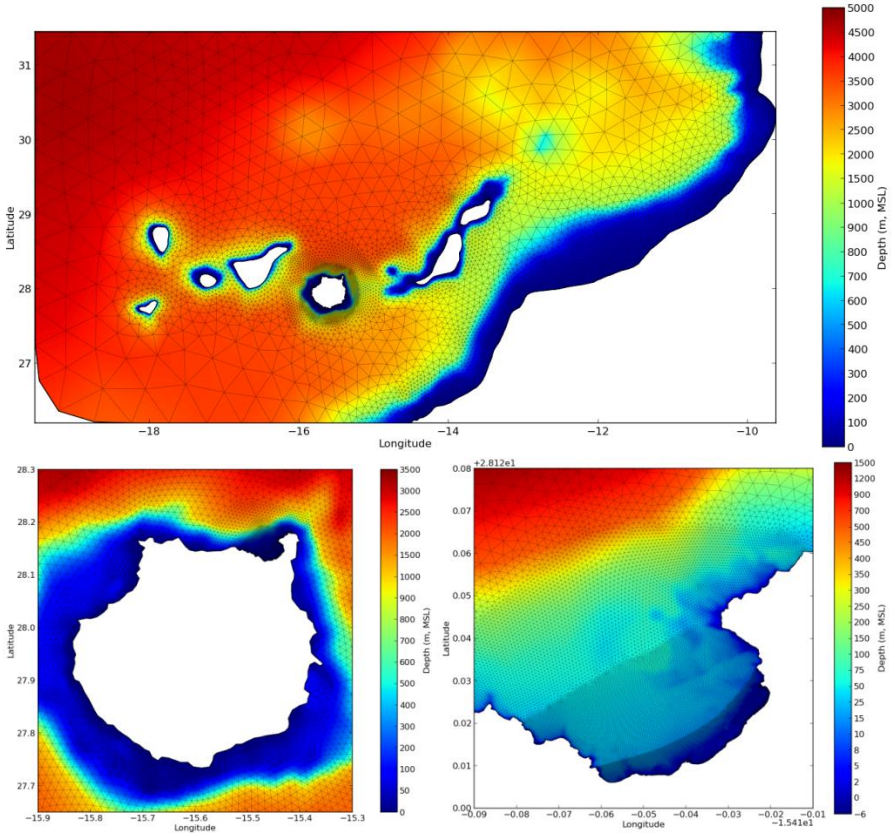


*Figure 12:Bathymetry and grid from the study domain (top), Gran Canaria Island (bottom left) and Confital Bay (bottom right).*

## 4.3. Boundary and initial conditions

Tidal conditions were imposed at the open boundary nodes. Twenty-three tidal constituents were considered based on the regional circulation model of Fortunato et al. (2016): Z0, SSA, MM, MF, MSf, O1, K1, P1, Q1, N2, M2, S2, K2, 2N2, Mu2, Nu2, L2, M3, MN4, M4, MS4, M6, and2MS6. The following table (Table 3) collects the constituents within their amplitude and phase values used for the 31 days validation run (in section 4.4). Atmospheric forcing, namely

wind, was also considered using NCEP/NCAR reanalysis data. Initial conditions were also established for temperature (24°C) and salinity (35 psu).

*Table 3: Tidal constituents.*

| Constituent | frequency (rd/s) | Amplitude factor | Nodal angle (phase) | Description |
|---|---|---|---|---|
| **Z0** | 0.00000E+00 | 1.00000 | 0.00 | Equilibrium reference to MSL |
| **SSA** | 0.3982127623E-06 | 1.00000 | 319.69 | Solar semiannual constituent |
| **MM** | 0.2639203103E-05 | 1.13122 | 6.33 | Lunar monthly constituent |
| **MF** | 0.5323414371E-05 | 0.62534 | 14.83 | Lunisolar fortnightly constituent |
| **MSf** | 0.49252122E-05 | 1.03777 | 54.47 | Lunisolar synodicfortnightly constituent |
| **O1** | 0.6759774260E-04 | 0.80600 | 49.04 | Lunar diurnal constituent |
| **K1** | 0.7292116061E-04 | 1.03777 | 299.25 | Lunar diurnal constituent |
| **P1** | 0.7252294745E-04 | 1.00000 | 110.15 | Solar diurnal constituent |
| **Q1** | 0.6495854177E-04 | 0.80600 | 49.04 | Larger lunar elliptic diurnal constituent |
| **N2** | 0.1378797024E-03 | 1.03777 | 299.25 | Larger lunar elliptic semidiurnal constituent |
| **M2** | 0.1405188959E-03 | 1.03777 | 305.57 | Principal lunar semidiurnal constituent |
| **S2** | 0.1454441081E-03 | 1.00000 | 0.00 | Principal solar semidiurnal constituent |
| **K2** | 0.1458423212E-03 | 0.74725 | 320.10 | Lunisolar semidiurnal constituent |
| **2N2** | 0.1352404942E-03 | 1.03777 | 292.92 | Lunar elliptical semidiurnal second-order constituent |
| **Mu2** | 0.1355936984E-03 | 1.03777 | 251.10 | Variational constituent |
| **Nu2** | 0.1382329065E-03 | 1.03777 | 257.42 | Larger lunar evectional constituent |
| **L2** | 0.1431581040E-03 | 0.00000 | 130.86 | Smaller lunar elliptic semidiurnal constituent |
| **M3** | 0.2107783439E-03 | 1.05729 | 278.36 | Lunar terdiurnal constituent |
| **MN4** | 0.2783985983E-03 | 1.07697 | 244.82 | Shallow -water quarter diurnal constituent |
| **M4** | 0.2810377918E-03 | 1.07697 | 251.14 | Shallow -water overtides of principal lunar constituent |
| **MS4** | 0.2859630040E-03 | 1.03777 | 305.57 | Shallow -water quarter diurnal constituent |
| **M6** | 0.4215566877E-03 | 1.11766 | 196.71 | Shallow- water overtides of principal lunar constituent |
| **2MS6** | 0.4264818999E-03 | 1.07697 | 251.14 | Shallow-watersixthdiurnal constituent |

## 4.4. Model Validation

The model was forced by tidal constituents (Table 3) and atmospheric forcing along a period of 31 days of simulation, starting on September 1$^{st}$ of 2015.Model results of different parameters (sea level, Eulerian current magnitude and direction, and Lagrangians trajectories) where compared with field observations to evaluate the accuracy of the model predictions.

### 4.4.1. Sea level validation

The simulated surface water levels were validated through the comparison with hourly sea level elevations measured by the tide gauge of Las Palmas Port (Figure 13). The estimated root mean square error between both time series (real measures and model results) was approximately 7 cm and lower than 6 cm without accounting the mean.

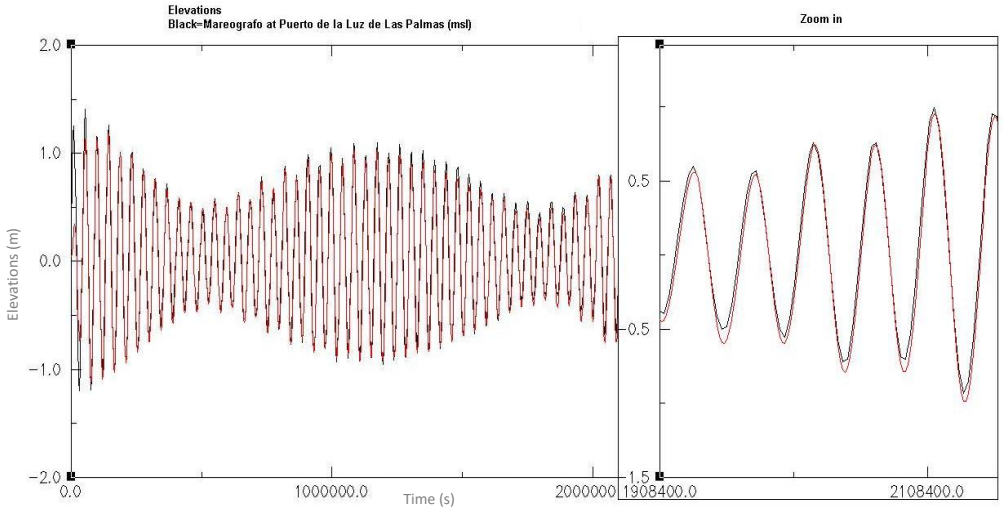


*Figure 13: Sea level elevations (in meters) on the vertical axis and time (in seconds) on the horizontal. Tide gauge measurements (black) and SCHISM model results (red). Right plot shows a zoom in of the elevations.*

### 4.4.2. Current validation

- *Eulerian current validation*

The magnitude and direction of the simulated currents were validated with the observations obtained from the Eulerian current meter placed in the study area (section 3.2.2.). Due to the small period of available data, the validation was only possible for that short time. The data measured by the current meter were previously filtered by a running average filter with a specific width of 3 data, as a result, the standard deviation of both raw and filtered data was of 4.3 cm and 3.9 cm respectively. The error of the current magnitude between the filtered data from the Aquadopp and the model results was about 6 cm/s.

The current magnitude was better represented by the model than the direction. The model was not able to represent adequately the observed peaks. Figure 14 shows the current velocity measured by the current meter and the predicted by the model. The difference observed may be related with other forces such as waves or local fluctuations of wind, which are not considered in the model. The wind forcing, in particular, has a low temporal resolution (6 hours), while the currents were measured every twenty minutes. As a result, the variations in the current in that time interval would not be captured by the model. Regarding to the current direction results the model was unable to represent the smaller oscillations, although the main real direction behaviour was captured by the model.

Despite all the difficulties mentioned, the model was able to represents the main patterns of circulation relevants for the purpose of this work, which allowed the development of the remaining established points.

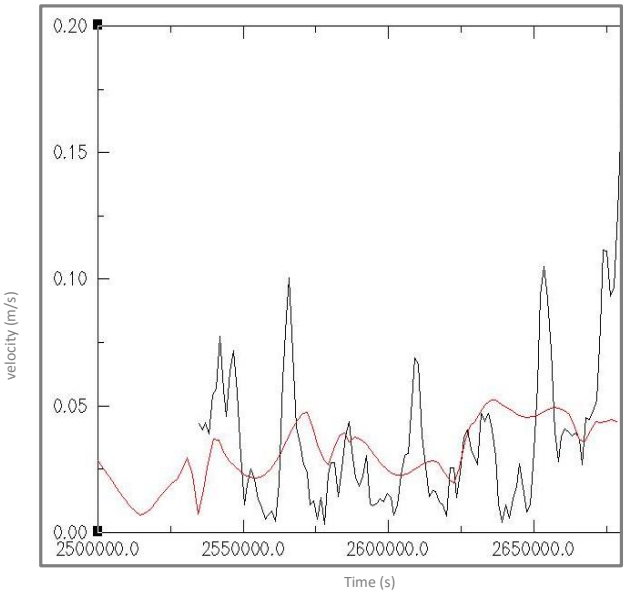


*Figure 14:Eulerian current measure (black) and model simulation result (red). Vertical axes represent the velocity (in m/s), and horizontal the time (in seconds) started on the 1st of September 2015.*

- *Lagrangian current validation*

The three-dimensional particle-tracking model available within SCHISM system was applied to compare the model predictions with the drifter data measured at Las Canteras Beach. Simulations were performed for the specific days on which the drifters were in the water. Although this section was very ambitious and interesting, the lack of time prevented a deeper analysis and only the measurements from the 17$^{th}$ of July 2015 were validated. The wind and tide conditions were set-up in the same way than in section 4.4.2. Tidal and wind forcings conditions were updated for the simulated period, following a similar approach to the one described in section 4.3. Simulated elevations and three-dimensional velocities were used to force the particle tracking model. Both drifters and model results were plotted together to validate the simulations. Several complications occurred such as the very short measurements periods of the drifters, which resulted in very little time coincidence within the model runs. The time intervals during the field data acquisition did not exceed one hour, while the model outputs were set for longer time steps. The adaptation of these outputs to shorter times steps required more time than what the student had left.

Results showed a common transport pattern (Figure 15), although some differences existed, namely higher velocities in the modelled particles than in the observations. These differences may be due to the points discussed previously. The difference between the SCHISM pasive particles, which where set-on the surface waters, and the drifters, which are driven by currents (30-40 cm) below the surface and could result in a lower speed of transport, may also explain soe of the differences. Overall, the main direction and trajectories were represented by the model, recreating real situations of surface particles transport.

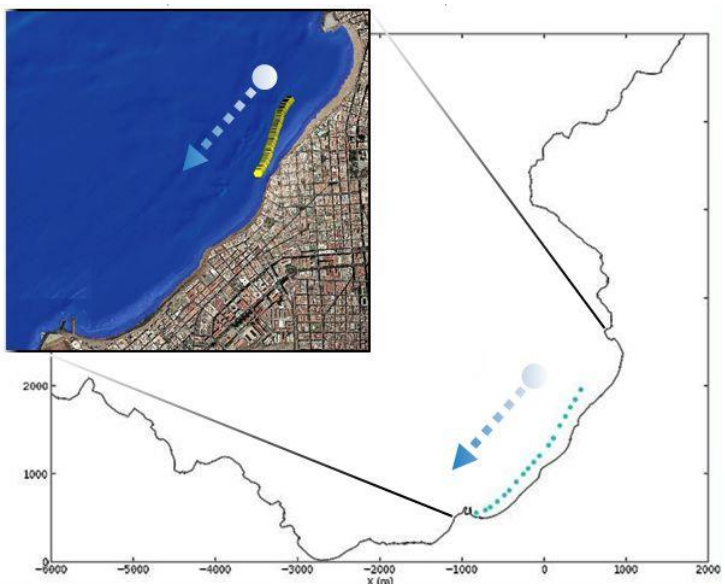


*Figure 15: Lagrangian current validation. In yellow drifter measure (start at 9:07on 17th July 2015), in blue langrangia trajectory model result. The arrow shows the direction of the trajectories.*

## 4.5. Wind scenarios

The next step developed was the simulation of different wind scenarios, which may influence the circulation patterns in the study area. To define these scenarios, the most frequent wind directional sectors were identified through the observations of the reanalysis results at a point near the study area from the HIPOCAS project (see section 3.2.4). Figure 16 shows the most frequent wind directions registered. Accordingly, the chosen wind scenarios were NNE, N, NE and NNW, and the wind speed, 5m/s.

The simulations of the four wind scenarios were carried out through equilibrium tidal conditions, only the principal semidiurnal components were considered (M2 and S2), to minimize variables and easily reach the circulation behavior from each wind direction. Each synthetic simulation lasted 18 days. From each wind scenario, the resultant residual current direction and maximum velocity field were analyzed to characterize the circulation pattern.

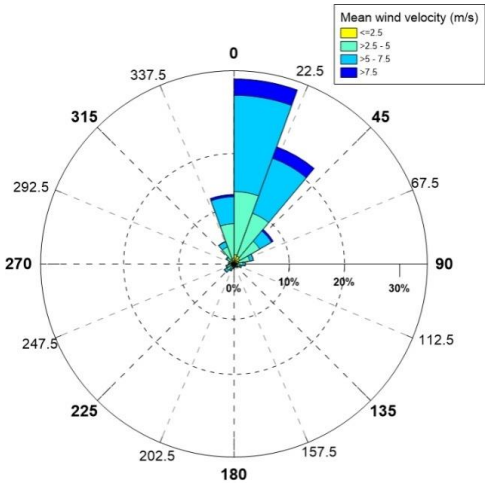


*Figure 16: Wind rose from atmospherics reanalysis point located near to Confital Bay from 1958-2000.*

## 4.6. Lagrangians particle simulations

The Lagrangian simulations aimed to simulate the particle pathways. This was accomplished by the application two models, VELApart (2D) and SCHISM (3D) (section 4.4.). The reasons for the use of the Lagrangian models were the possibility to perform backwards simulations to establish a possible origin, transport and accumulation of the debris, and the validation of the model with the comparison between simulated particles and the drifters data.

### 4.6.1. VELApart beach release

The two and quasi-three-dimensional VELApart model was applied to simulate the pathways of particles in surface waters. In the 2D version, the model solves the advection-diffusion equation in Lagrangian form for individual, passive, and non-reactive particles, forced by a depth-averaged velocity field, which was extracted from the resultant current field of SCHISM simulations. Although the original idea was the use of the backward setup, only the 2D forward simulation was implemented due to complications and lack of time for its proper application. Therefore, for the application of this model, the velocity fields previously calculated from the wind scenarios simulations of SCHISM (section 4.5.), were used to force the VELApart model and simulate the trajectories of the particles in the surface. This is illustrative because the simulations were done with the resultant current from the synthetic runs under constant winds conditions and equilibrium tide. Apart from this, the results complement the previous observations on the Lagrangian current validation.

A total of 200 artificial passive particles were released in the study domain, along the coastline of Las Canteras beach at a bathymetric line of 2.20 meters, and whose different winds influence trajectories were traced. The model ran with a tracking error criterion of 0.1 cm and a horizontal constant diffusion of 0.03 $m^2/s$. This horizontal constant diffusion was approximately obtained after consideringthe distance on which a single particle would covered after 1 hour through diffusion, on which it was accorded to be 25 m. These simulations helped to understand the possible paths that particles would follow under different wind conditions (NNE, N, NE and NNW). The simulations were carried out with a 5 minutes time steps for almost 70 days of simulations.

# 5. Results and discussion

## 5.1. Marine debris

### 5.1.1. Meso- and micro-debris results

The analysis of meso- and micro-debris characteristics collected in the three selected transects reveals that the density of is lower at Tr1 (La Puntilla) and increases toward Tr3 (La Cicer) (see Figure 17). Averaging the observations obtained through the year (seven surveys) reveals that Tr3 remains the transect with the highest values while Tr1 and Tr2 present similar average values. Nevertheless, it is important to note that mean and standard deviation values are of the same order (Table 4). This similarity implies a large variability in the number of item per

transect observed throughout the year. However, a study of annual patterns cannot be addressed due to the limitation imposed by the observation period.

Regarding the type of materials found per transect (Figure 18, left), it can be observed that fragments type is the most frequent type of materials found in any transect. Transect Tr1 suspiciously receives much more line type (which are basically mono-lines of nylon) than in any other transect. This could be related with main fishing-related activities developed in the proximities. In terms of materials size (Figure 18, right), the range of diameters between 1.4 and 4 mm is predominant in all transects. Nevertheless, Tr1 differs from the other two transects by receiving more small size items, while Tr2 and Tr3 have similar proportion for this size range. Furthermore, there is a notable increase from Tr1 to Tr3 in the percentage of middle size (4-9 mm) while the relative amount of higher items (9-25 mm) slightly decreases.

*Table 4: Average and Standard deviation of Items/m² per transect.*

| | Tr1 | Tr2 | Tr3 |
|---|---|---|---|
| **Average** | 15 | 19 | 70 |
| **Standard deviation** | 16 | 19 | 79 |

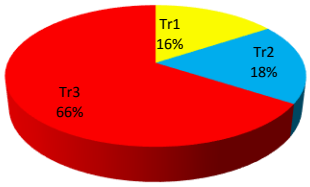


*Figure 17: Percentage of items/m² of meso- and micro- debris per transect.*

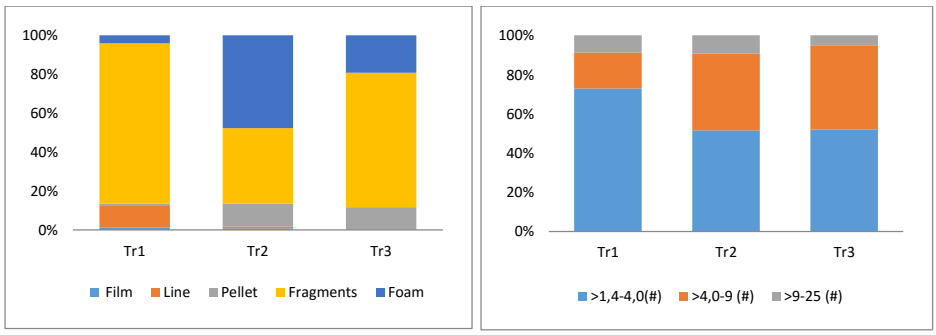


*Figure 18: Type of materials rate per transect (left) and size range per transect (right).*

### 5.1.2. Macro-debris

This section presents the results of macro-debris found for the three transects. The overall behavior found was a higher presence of debris on Tr3, La Cicer, although this result was obtained through the comparison between different groups of debris (see Figure 19), where three pie charts are represented. Considering only the total amount of items, (Figure 19 (a)), Tr2 is the most polluted transect, although, as it can be seen in Figure 19 (b), taking into account only synthetic materials, Tr3 is by far the most polluted transect. This

misunderstanding is the result of the great presence of cigarette filters sampled on Tr2 (Figure 19 (c)). The Tr2 transect holds more cigarette filters than any other. This finding suggests a particular type of user on this beach area. The average and standard deviation values per each transect are given in Table 5. In terms of average items per transect, Tr2 and Tr3 are the areas where more debris are found. The small standard deviation of Tr2 indicates the more frequent encounter of debris at this site than in any other transect, although, as it was commented, this may result of continuous pollution due to smoker beach user.

The main composition of synthetic items per transect is represented in Figure 20. The graph shows a clear majority of hard plastic items on all the transects, being this synthetic material type the most abundant, followed by plastic films, foamed plastic and rubber.

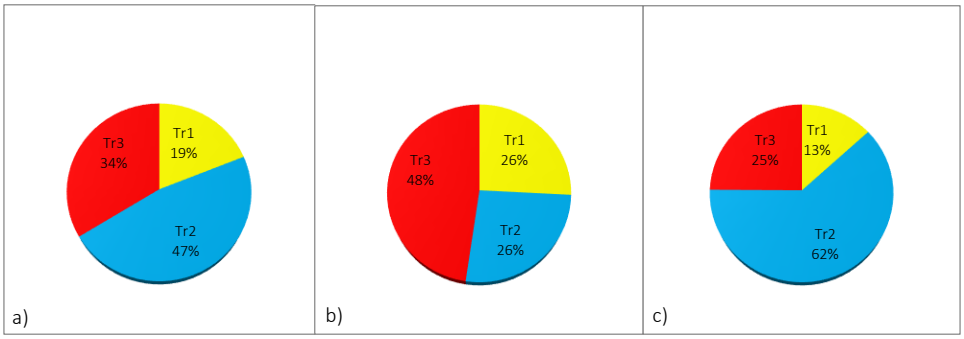


*Figure 19: Total debris per transect (a), total synthetic debris per transect (b), total cigarette filters per transect (c).*

*Table 5: Average and Standard deviation of total Items/100m2 per transect.*

| | Tr1 | Tr2 | Tr3 |
|---|---|---|---|
| **Average** | 51 | 128 | 91 |
| **Standard deviation** | 58 | 39 | 48 |

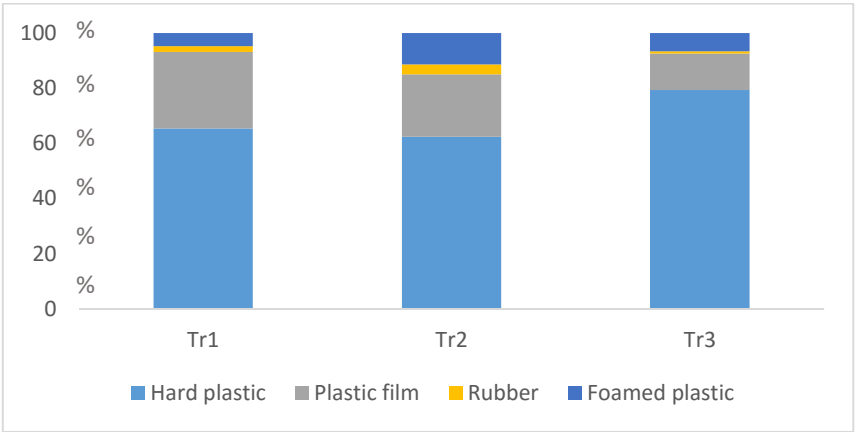


*Figure 20: Percentage of synthetic main groups items per transect.*

Due to the great abundance of the hard plastic group, the percentage of each subgroup (see section 3.1.2.) on all transects are represented onTable 6. From the hard plastic group, the pieces subgroup (A15) constitutes the main type of material found on Tr2 and Tr3, and plastic

nets-ropes (A11) for Tr1. As it was mentioned in the classification description, A11 items are typically items used on fishing-related activities. As a result, Tr1 is highly influenced by marine source debris, or at least by fishing related activities.

To address a possible signs of marine source materials, of bites or biofouling marks, as related-activities materials, was taken into account. Table 7 shows the percentage of total items per transect, and groups of materials, where its possible marine origin was able to address. The transects on the limits, such as Tr1 and Tr3, showed higher of these visible signs on materials, in terms of total debris or synthetic materials type. Nevertheless, the Tr2 transect only held the majority of marine signs on cigarette filters group, which is expected due to the great amount of these items found this section of the beach (Figure 19, c)).

*Table 6: Percentage of Hard plastic sub groups items per transects.*

| | TR1(%) | TR2(%) | TR3(%) |
|---|---|---|---|
| **A11** | 62 | 12 | 12 |
| **A12** | 1 | 2 | 0 |
| **A13** | 9 | 30 | 19 |
| **A14** | 3 | 10 | 13 |
| **A15** | 25 | 44 | 55 |
| **A17** | 0 | 0 | 0 |
| **A18** | 0 | 3 | 1 |

*Table 7: Percentage of possible marine source, not locally disposed, of materials.*

| | Total debris (%) | Synthetic debris (%) | Cigarette filters (%) |
|---|---|---|---|
| **Tr1** | 45 | 58 | 27 |
| **Tr2** | 34 | 50 | 30 |
| **Tr3** | 50 | 68 | 29 |

## 5.2. Current patterns under different wind/tidal scenarios results

### 5.2.1. NNE and NE scenario

The direction and magnitude of the residual currents and maximum velocity (Figure 21 and Figure 22 respectively) for the NNE (23°) and NE (45°) wind scenarios (5 m/s) are presented next.

Resultant residual currents in El Confital Bay for two different wind scenarios are shown in Figure 21 Wind conditions are represented by homogeneous wind fields blowing at 5 m/s from NNE and NE, respectively. Note that these conditions represent very frequent situations in the study area.

The residual current field obtained outside of the bay for a wind field from NNE (Figure 21,left) shows a circulation pattern towards the west but significantly intensified at the northeast cape delimiting the bay, where the flux is also directed towards the bay in southwest direction. Current intensity is rather weak in the main part of the bay and mainly flowing westwards.

Flow enters to the inner part of the bay, between the rocky-reef and the beach, through the narrow opening left by the reef at its northeast extreme. In this nearshore area the flow is accelerated toward the opposite extreme of the beach, where the rocky-reef disappear (groynes) along the narrow channel formed between the reef and the beach. Then, water flows northwest along the coast.

Current field under the NE wind conditions shows a similar pattern to that observed for NNE wind (Figure 21, right). Nevertheless, some significant differences can be observed, including a flow enhancement of the transport into the west and a reduction of the transport into the bay, thus decreasing the flow speed in the nearshore zone. It is interesting to highlight the acceleration experienced by the flow in the nearshore areas between the three openings left by the rocky-reef, where the water depth reduces.

Maximum current velocity fields corresponding to the above discussed wind field directions are shown in Figure 22. Patterns commented above are also clear, observed in this figure for both cases. However, there are some aspects to remark. One of these is the existence of a broad area of calm waters in the north limit of the beach, where transect Tr3 is located, used as a refuge for small fishing and recreational boats. Transect Tr2 is located in a zone where flow is accelerated, while area of Tr3 is always exposed to wave action and longshore current intensity reduces. Zones of maximum intensity flow are located in shallow areas above mentioned, north and south of the middle opening in the reef. Nevertheless, Figure 22 reveals a significant intensification of flow in the southern limit of the beach (groynes). Area of lower flow could indicate possible zones where marine debris accumulation is more probable to occur. On the other hand, as the main current direction flow towards the south end of the beach, it seems reasonable to expect that larger amounts of debris could be found here, because of the transport of materials along the nearshore channel and the barrier imposed by the groynes. The main differences between both scenarios results are higher values of maximum velocity for NE wind on the southern limit of the beach (by the groynes) and a higher value for NNE in the nearby of transect Tr2.

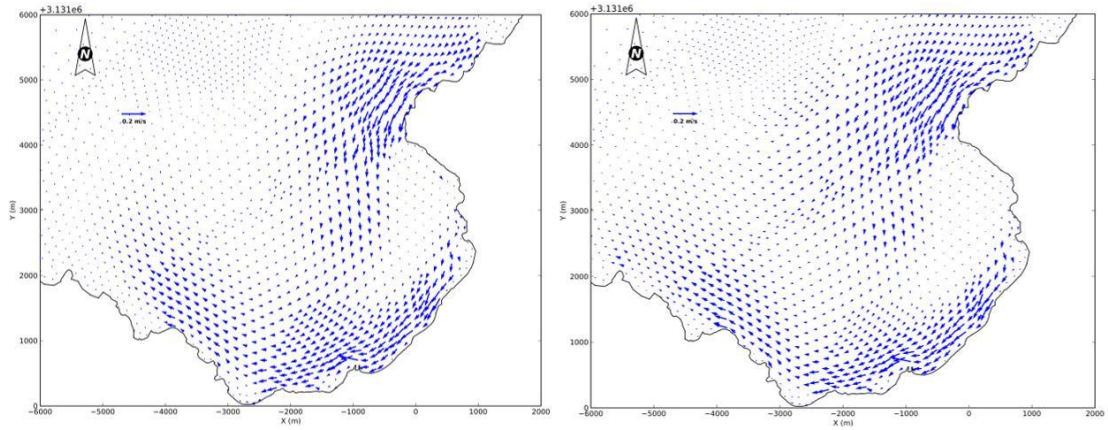


*Figure 21: Residual currents for the NNE (left) and NE (right) wind scenarios.*

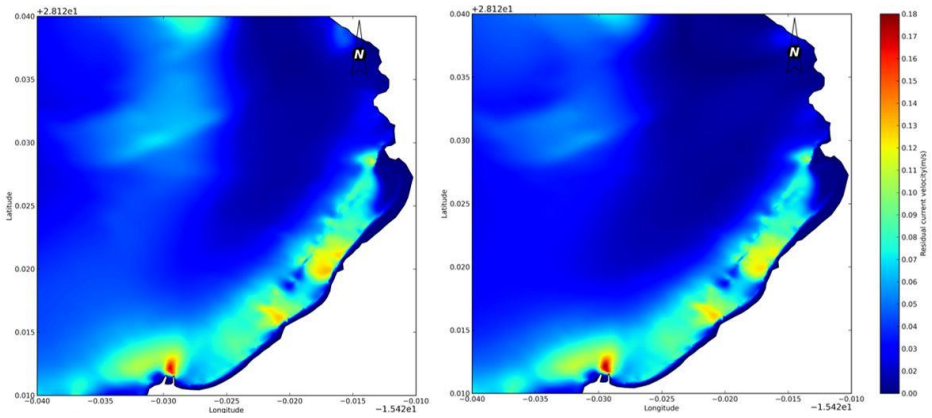


*Figure 22: Maximum velocity field from NNE (left) and NE (right) wind scenarios at Las Canteras Beach.*

### 5.2.2. N and NNW scenario

Resultant residual current direction and magnitude for the North (0°) and North-northwest (338°) wind scenarios are shown in Figure 23, while maximum current velocity field are depicted in Figure 24. As in the previous section, these current fields were obtained by using as input a constant wind direction (N and NNW, Figure 23 left and right, respectively) and a constant speed of 5 m/s.

Both wind scenarios show a recirculation pattern in the eastern-central of the bay a converge behavior of the residual current circulation among the eastern side of the bay. The main transport direction is not as clear as previous scenarios. The N wind direction (Figure 23, left) still showed an overall tendency of transport towards the west, although, with an opened trajectory away from the coast when the southern limit of the beach is reached. On the other hand, NNW wind (Figure 23, right) illustrate a stronger converge behavior, giving a sense of a more circular pattern transport in the entire bay. The main transport direction of NNW scenario is less clear, receiving SE flow from the north coast, and a stronger recirculation along the eastern side of the bay.

Although the last noticeable behavior seems to push away the possible debris contained in the surface waters, it cannot be ignored the possible increase of exposure of these materials with the intrusion and the light recirculation of the current on the entire beach.

Regarding to the maximum velocity current results, the higher values are located on the same protrusion edges cited on the previous scenarios but with lower values (Figure 24), especially for NNW scenario (Figure 24, right). As a result, disperse lower energy areas occur under these wind condition and its possible effects with debris deposition should carefully considered. Because of the particular behavior of NNW wind, an extra similar wind scenario was taken into account, the NW (315°) wind direction, to come up with other highly vulnerable conditions that could produce higher amounts of stranding materials in the study area.

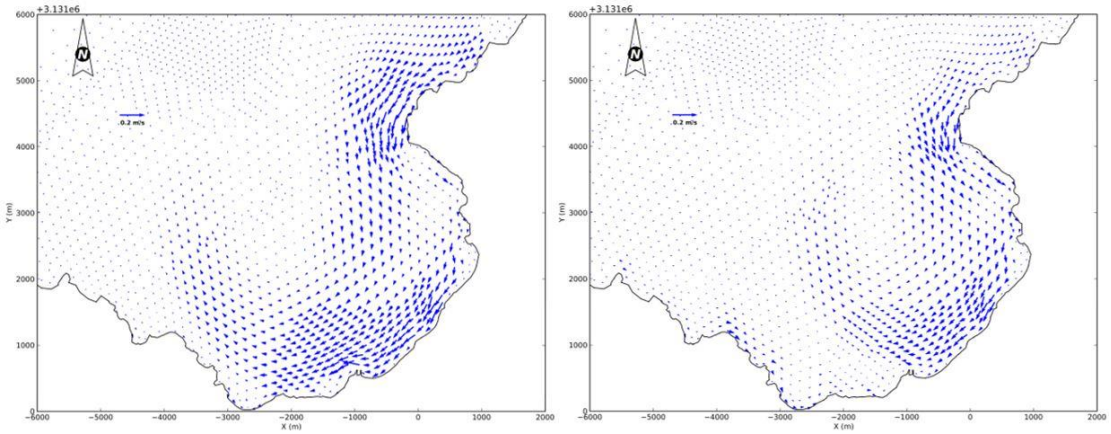

*Figure 23: Residual currents for the N (left) and NNW (right) wind scenarios.*

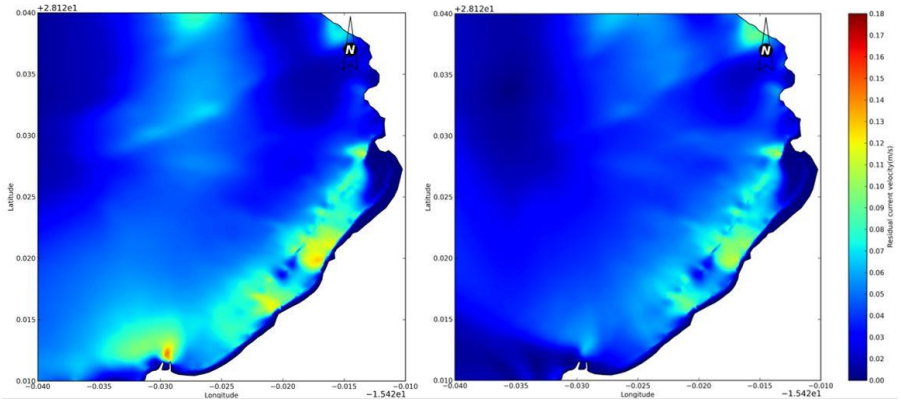

*Figure 24: Maximum velocity current field from N (left) and NNW (right) wind scenarios at Las Canteras Beach.*

### 5.2.3. Extra wind direction observation

To account for all the wind directions that may potentially have negative consequences in the area, the NW (315°) scenario was also analyzed. The simulation and residual calculation was done under the same conditions than in the other synthetic simulations (described in section 4), namely considering a constant velocity of 5 m/s and equilibrium tides at the oceanic boundary.

The circulation pattern observed under this wind conditions results very interesting. It can be observed (Figure 25) that currents along the northeast and southwest flanks of the Bay are directed towards the beach, entering into the channel between the barrier and the beach through the barrier openings at the beach north and south limits. These flows turn to the opposite beach ends and collide close to the central opening of the barrier, where longshore current component decreases, inducing a seaward recirculation. Furthermore, the returning flow shifts eastwards and its combination with the flow incoming along the northeast size generates a recirculation cell in the eastern-central part of the bay (Figure 25).

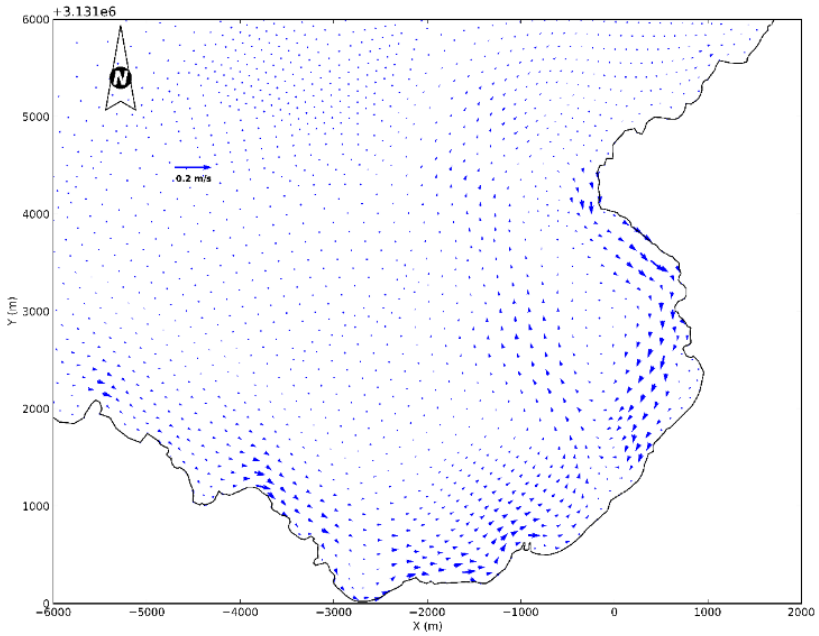


*Figure 25: Residual current NW (315°) wind scenarios.*

Under this condition, the possible accumulation of marine debris in the beach, especially at "Peña la vieja" section could be much more noticeable than in other wind scenarios. The push of the surface water from the north coastline to the beach of Las Canteras, and also the recirculation produced on the eastern side of the bay, would probably cause a larger deposition.

## 5.3. Lagrangians particle simulations

Langrangian simulations were developed to simulate particle tracking and were accomplished throughout two models, Velapart (2D) and SCHISM (3D). Lagrangian models enables to carry out backwards simulations, thus offering the possibility to explore the location of possible debris source and sink points, as well as transport paths, in addition to its usefulness for model validation by the comparison between simulated particle and drifters paths.

### 5.3.1. VELApart

Two main transport behaviors can be distinguished. One related to conditions of wind blowing from the directional sectors NE-NNE and other associated to N-NNW wind directions. Winds blowing from NE and NNE sectors tend to transport the particles along the beach towards its south limit and then along the north-west coastline. This transport may be interrupted by the physical barriers or coastline morphologies oriented towards the NE found along the way. N-NNW but particularly NNW winds, tend to promote the recirculation of the particles in the Confital Bay, such as previously indicated. In this sense, further research regarding the influence of the winds from the N-NNW, and probably from NW too, should be performed to analyze in more detail the observed behavior. In the presence of marine debris, this current pattern could enhance the debris deposition, or even trap it, inside this environment. Pathways of the particles for almost two days of simulation are represented in Figure 26 and clearly show the previous comments.

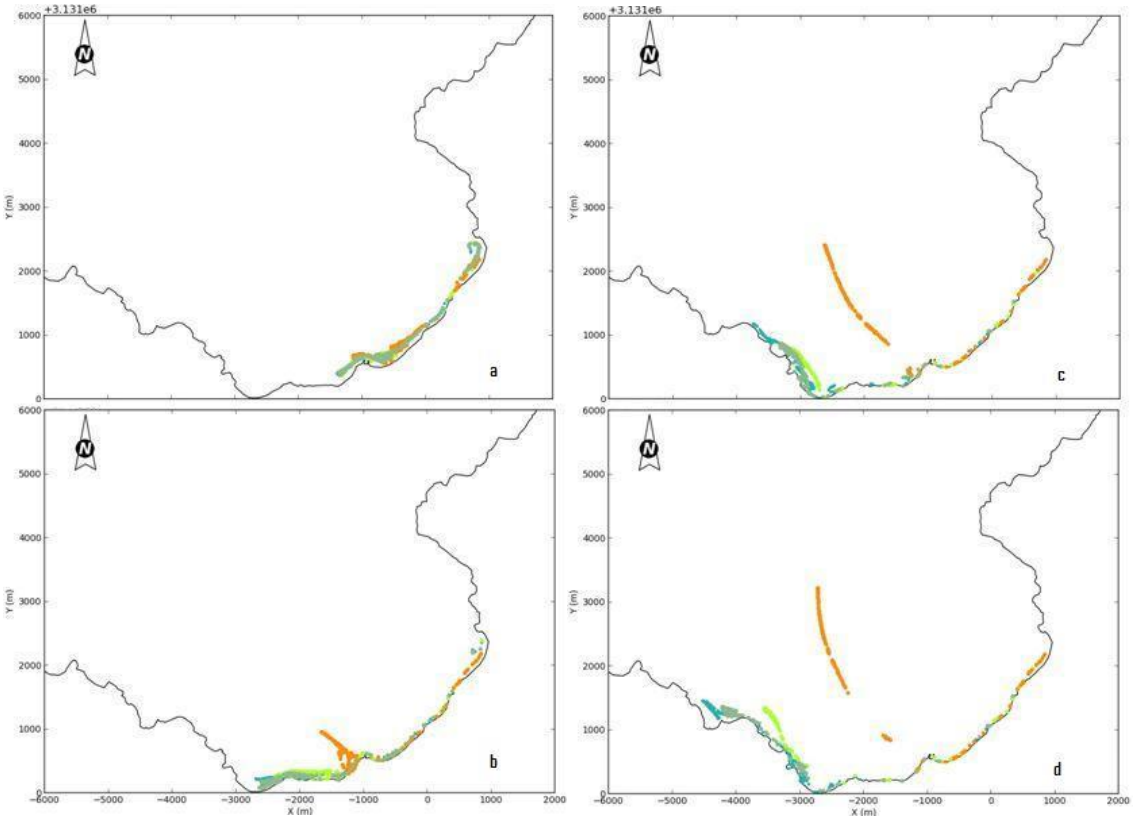


*Figure 26: Times 4.58h (a), 14.58h (b), 29.58h (c), and 39.58h (d).Winds from NE (blue), NNE (grey), N (green), and NNW (orange).*

### 5.3.2. Particle tracking for extra wind scenario results

As previously commented, NW wind conditions induces a very specific current pattern in the study area. Figure 27 shows the influence of NW wind on the surface trajectories of the artificial particles. The times chosen cover a period of 13 days to complete the full recirculation pattern between the northern and middle openings of the barrier. This lead to particular awareness due to the higher probabilities of marine debris recirculation and possible deposition, if similar wind conditions occur.

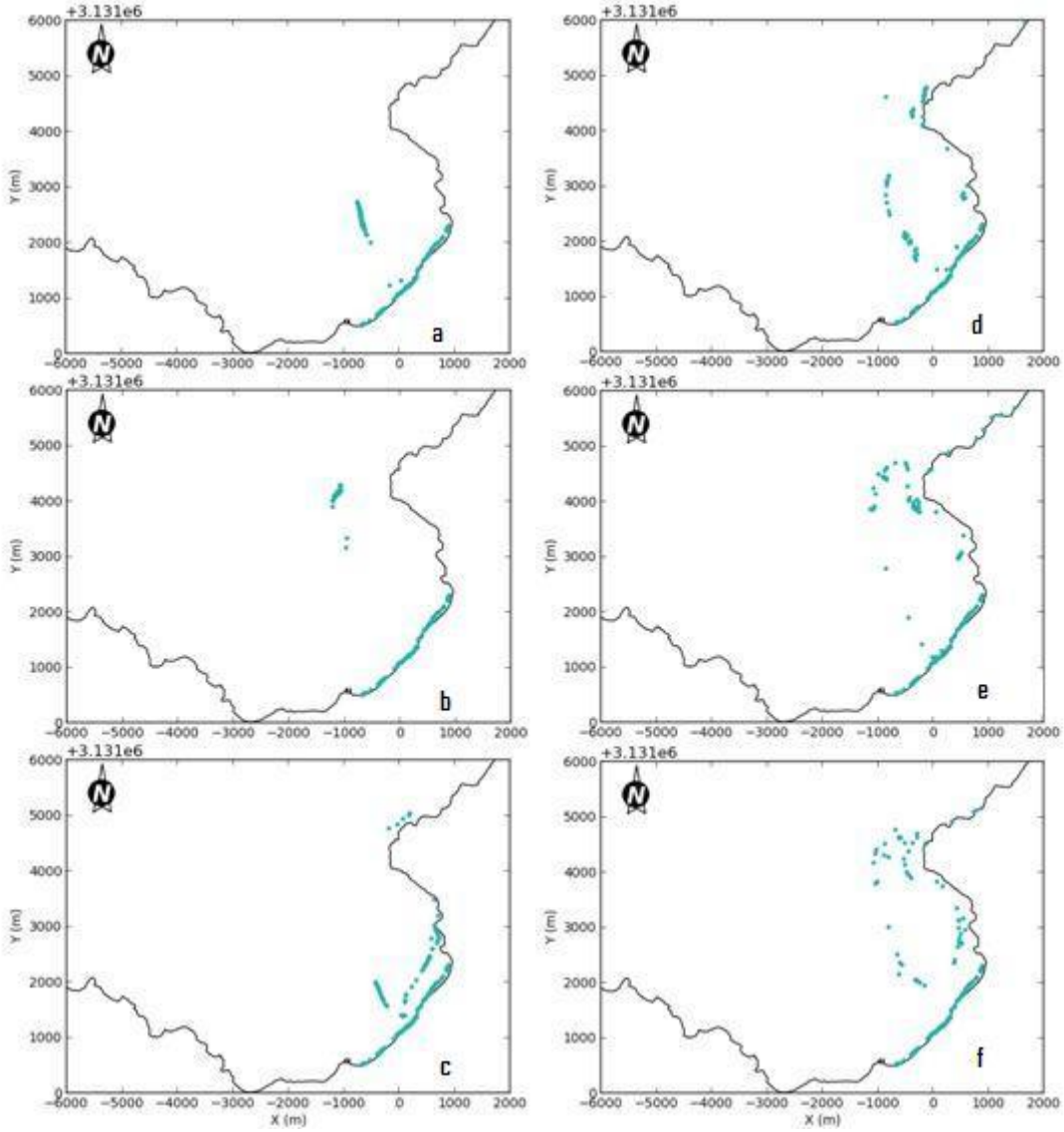


*Figure 27:Wind coming from NW (315°) particle simulation. Times 24.58h (a), 44.58h (b), 94.58h (c), 179.58h (d), 229.58h (e), and 314.58h (f).*

# 6. Conclusions

Meso- and micro-debris amount collected on the beach surface is lower on the northern limit of the beach and increases toward its southern part. Nevertheless, there is a significant variability in the number of items observed at each transect throughout the year.

The fragments type of plastic debris is the most frequent in any transect. Transect Tr1 receives much more line type than in any other transect, which could be related with main fishing-related activities developed in the surroundings of this transect. Material belonging to the size range between 1.4 and 4 mm is predominant in all the transects. Nevertheless, Tr1 differentiates from the other two by receiving larger amounts of small size items, while the proportion received at these transect (Tr2 and Tr3) is similar.

In relation to Macro-debris, the higher amount is found at Tr3. However, considering only the number of items, Tr2 is the most polluted transect while, taking into account only synthetic materials Tr3, is by far the most polluted. This confusing result is due to the important contribution of cigarette filters type material observed at the middle transect. The main composition of macro-synthetic items per transect hard plastic items represents the main contribution at all the transects.

NE and NNE wind conditions represent the most frequent situations in the study area. Residual currents for winds from NNE shows a main circulation pattern directed towards the west but significantly intensified at the northeast side of the bay, where the flux is also directed towards the bay in southwest direction. Current intensity is rather weak in the main part of the bay and mainly flowing westwards. Flow enters to the inner part of the bay, between the rocky-reef and the beach, through the narrow opening left by the barrier at its northeast extreme. In this nearshore area the flow is accelerated toward the opposite extreme of the beach, where the rocky-reef disappear (groynes) along the narrow channel formed between the reef and the beach. Then, water flows northwest along the coast. Circulation under NE wind conditions exhibit a similar pattern. Nevertheless, a transport enhancement into the west and a reduction of the transport into the bay, thus decreasing the flow speed in the nearshore zone, are observed. Furthermore, the flow in the nearshore areas between the three openings left by the rocky-reef, where the water depth reduces, is accelerated.

Circulation under N and NNW wind scenarios shows a recirculation pattern in the eastern-central part of the bay. The main transport direction is not so clear as in previous scenarios. For N wind conditions there is also an overall tendency of transport towards the west, although, with an opened trajectory away from the coast when the southern limit of the beach is reached. On the other hand, NNW wind conditions induce a more closed circulation pattern in the entire bay. The main transport direction of NNW scenario is less clear, receiving SE flow from the north coast, and a stronger recirculation along the eastern side of the bay. A similar behavior is observed in the maximum velocity fields for winds from N and NNW conditions. although larger areas of low energy are observed under NNW wind conditions.

NW wind conditions induce currents along the northeast and southwest flanks of the Bay directed towards the beach, entering into the channel between the barrier and the beach through the barrier openings at the beach north and south limits. These flows turn to the opposite beach ends and collide close to the central opening of the barrier, where longshore current component decreases, inducing a seaward recirculation. Furthermore, the returning flow shifts eastwards and its combination with the flow incoming along the northeast size generates a recirculation cell in the eastern-central part of the bay.

Two main transport behaviors can be distinguished in terms of the passive tracer pathways simulations. For winds blowing from the NE-NNE sector particles are pushed along the beach towards its south limit and then along the north-west coastline. This transport may be interrupted by the physical barriers or coastline morphologies oriented towards the NE. On the other hand, N-NNW wind conditions, particularly those from NNW may promote the recirculation of the particles in northeastern part of the bay.

NW wind conditions induce a very specific current pattern, by forcing a complete full recirculation between the northern and middle opening of the barrier.

Wind scenarios in the NNW-NE sector, used to simulate current fields in the study area, represent 90 %, approximately, of wind conditions observed during more than 40 years. The overall behavior of the current fields simulated induces a transport towards the west along the northern coast. These results seem to resemble the observed pattern of marine debris deposition, which is higher on the southern limit of the beach (Tr3). During the much less frequent NW wind scenario, forced pathways of particles describe a recirculation behavior which could have important implications on marine debris deposition.

Much more efforts are necessary to reach an adequate comprenhension of the relationships between coastal hydrodynamics and marine debris nearshore transport and deposition on beaches, due to the large number of factors involved and the resulting complexity of the process.

***Acknowledgements***

The present work would not have been possible without the support of the supervisors Germán Rodríguez Rodríguez, Marta Rodrigues and André B. Fortunato. Also special thanks to the Applied Marine Physics and Remote Sensing group (FIMATA) for providing me access to the necessary resources for developing this work, and to the Laboratório Nacional de Engenharia Civil (LNEC) for giving the opportunity of the internship. The sampling and measurement surveys would not have either possible without the help of friends and colleagues: Guilherme Clarindo Marcos, Francisco Javier Aguilar, Belén Areitio, Alberto Fernández López, Justine Laurent and Clément, Paula Mcknight Morales and Selene Radicci Reyes. Thanks to Oswaldo López (INNOVA) for providing help with measuring devices, Alejandro Marrero González and colleagues from California Sports Center (CSC), José Luis Samper and colleagues from Reprosub S.L, José (for his help at the laboratory), Peter (for always believing in me), Henry Carson (to inspire me), and JP (for that great tracking phone device). For kindly providing data and information: The Beach department of Las Palmas de Gran Canaria Council, Red Cross in Las Palmas, Puertos del Estado, and GEBCO.

This work is dedicated to my family, who have unconditionally supported me throughout my studies.

# 7. References

Barnes, D., Galgani, F., Thompson, R. and Barlaz, M. (2009). Accumulation and fragmentation of plastic debris in global environments. *Philosophical Transactions of the Royal Society B: Biological Sciences*, 364(1526), pp.1985-1998.

Baztan, J., Carrasco, A., Chouinard, O., Cleaud, M., Gabaldon, J., Huck, T., Jaffrès, L., Jorgensen, B., Miguelez, A., Paillard, C. and Vanderlinden, J. (2014). Protected areas in the Atlantic facing the hazards of micro-plastic pollution: First diagnosis of three islands in the Canary Current. *Marine Pollution Bulletin*, 80(1-2), pp.302-311.

Blickley, L., Currie, J. and Kaufman, G. (2016). Trends and drivers of debris accumulation on Maui shorelines: Implications for local mitigation strategies. *Marine Pollution Bulletin*, 105(1), pp.292-298.

Carson, H. (2013). The incidence of plastic ingestion by fishes: From the prey's perspective. *Marine Pollution Bulletin*, 74(1), pp.170-174.

Carson, H., Lamson, M., Nakashima, D., Toloumu, D., Hafner, J., Maximenko, N. and McDermid, K. (2013). Tracking the sources and sinks of local marine debris in Hawai'i. *Marine Environmental Research*, 84, pp.76-83.

Coe, J. and Rogers, D. (1997). Marine debris sources, impacts and solutions. *Springer*, New York, pp.432.

Critchell, K., Grech, A., Schlaefer, J., Andutta, F., Lambrechts, J., Wolanski, E. and Hamann, M. (2015). Modelling the fate of marine debris along a complex shoreline: Lessons from the Great Barrier Reef. *Estuarine, Coastal and Shelf Science*, 167, pp.414-426.

Derraik, J. (2002). The pollution of the marine environment by plastic debris: a review.*Marine Pollution Bulletin*, 44(9), pp.842-852.

EUROPARC (2014). EUROPARC-España, Anuario 2013 del estado de las áreas protegidas en España. Ed. *Fundación Fernando González Bermáldez*, Madrid, pp. 108.

Fortunato, A., Bruneau, N., Azevedo, A., Araújo, M.A.V.C., Oliveira, A. (2011). Automatic improvement of unstructured grids for coastal simulations, *Journal of Coastal Research*, Special Issue 64, pp.1028 - 1032.

Fortunato, A., Li, K., Bertin, X., Rodrigues, M. and Miguez, B. (2016). Determination of extreme sea levels along the Iberian Atlantic coast. *Ocean Engineering*, 111, pp.471-482.

Guedes Soares, C. (2008). Hindcast of Dynamic Processes of the Ocean and Coastal Areas of Europe. *Coastal Engineering*, 55(11), pp.825-826.

Hidalgo-Ruz, V., Gutow, L., Thompson, R. and Thiel, M. (2012). Microplastics in the Marine Environment: A Review of the Methods Used for Identification and Quantification.*Environmental Science & Technology*, 46(6), pp.3060-3075.

Isobe, A., Kubo, K., Tamura, Y., Kako, S., Nakashima, E. and Fujii, N. (2014). Selective transport of microplastics and mesoplastics by drifting in coastal waters. *Marine Pollution Bulletin*, 89(1-2), pp.324-330.

Ivar do Sul, J., Costa, M., Barletta, M. and Cysneiros, F. (2013). Pelagic microplastics around an archipelago of the Equatorial Atlantic. *Marine Pollution Bulletin*, 75(1-2), pp.305-309.

Ivar do Sul, J., Costa, M., Barletta, M. and Cysneiros, F. (2013). Pelagic microplastics around an archipelago of the Equatorial Atlantic. *Marine Pollution Bulletin*, 75(1-2), pp.305-309.

Jambeck, J., Geyer, R., Wilcox, C., Siegler, T., Perryman, M., Andrady, A., Narayan, R. and Law, K. (2015). Plastic waste inputs from land into the ocean. *Science*, 347(6223), pp.768-771.

Kalnay, E., Kanamitsu, M., Kistler, R., Collins, W., Deaven, D., Gandin, L., Iredell, M., Saha, S., White, G., Woollen, J., Zhu, Y., Leetmaa, A., Reynolds, R., Chelliah, M., Ebisuzaki, W., Higgins, W., Janowiak, J., Mo, K., Ropelewski, C., Wang, J., Jenne, R. and Joseph, D. (1996). The NCEP/NCAR 40-Year Reanalysis Project. *Bull. Amer. Meteor. Soc.*, 77(3), pp.437-471.

Laist, D. (1987). Overview of the biological effects of lost and discarded plastic debris in the marine environment. *Marine Pollution Bulletin*, 18(6), pp.319-326.

Lippiatt, S., Opfer, S., and Arthur, C.(2013).Marine Debris Monitoring and Assessment. NOAA *Technical Memorandum* NOS-OR&R-46.

Liubartseva, S., Coppini, G., Lecci, R. and Creti, S. (2016). Regional approach to modeling the transport of floating plastic debris in the Adriatic Sea. *Marine Pollution Bulletin*, 103(1-2), pp.115-127.

Magrama (2006) Ministerio de Agricultura, Alimentación y Medio Ambiente. Ecocartográfico, Demarcación de Costas. Costas: Arco Norte de Canarias, Proyecto 5582_02 Estudio Ecocartográfico del Norte de Gran Canaria. Bahía del Confital.

MARPOL (1973/1978) The international convention for the prevention of pollution from ships, 1973 as modified by the protocol of 1978, Annex V. Prevention of pollution by garbage from ships, entered into force, 31 Dec 1988.

Martínez, J., Alvarez, R., Alonso, I. and del Rosario, M. (1990). Analysis of sedimentary processes on Las Canteras beach (Las Palmas, Spain) for its planning and management. *Engineering Geology,* 29, pp.377-386.

Martínez, J., Gordo, C., Jimenez, J., Santana, J. and Veloso, J. (1988). Dinámica sedimentaria en la playa de Las Canteras (Las Palmas de Gran Canaria). *Revista de obras públicas*, pp.145-152.

Maximenko, N., Hafner, J. and Niiler, P. (2012). Pathways of marine debris derived from trajectories of Lagrangian drifters. *Marine Pollution Bulletin*, 65(1-3), pp.51-62.

McDermid, K. and McMullen, T. (2004). Quantitative analysis of small-plastic debris on beaches in the Hawaiian archipelago. *Marine Pollution Bulletin*, 48(7-8), pp.790-794.

Moore, C. (2008). Synthetic polymers in the marine environment: A rapidly increasing, long-term threat. *Environmental Research*, 108(2), pp.131-139.

Oliveira, A., Fortunato, A.,(2002). VELApart User's Manual: a Quasi-3D Particle Tracking Model for Shallow Water Simulations. Rep. 82/02-NET, LNEC.

OSPAR Commission (2010). Guideline for monitoring Marine littler on the beaches in the OSPAR maritime Area. London, UK: OSPAR Commission, pp.84.

REDMAR, Red de Mareografos de Puertos del Estado: Resumen de parámetros relacionados con el nivel del mar y la marea que afectan a las condiciones de diseño y explotación portuaria. Puerto de Las Palmas. Área de Medio Físico, Dirección Técnica- Puertos del Estado <www.puertos.es>

Rees, G. and Pond, K. (1995). Marine litter monitoring programmes—A review of methods with special reference to national surveys. *Marine Pollution Bulletin*, 30(2), pp.103-108.

Ribic, C., Sheavly, S. and Klavitter, J. (2012). Baseline for beached marine debris on Sand Island, Midway Atoll. *Marine Pollution Bulletin*, 64(8), pp.1726-1729.

Rodríguez, G., Clarindo, G. and Mcknight, L.(2015). Jellyfish outbreaks in coastal city beaches from a management perspective. *Coastal Cities and their Sustainable Future* 148, pp.277-288.

Ryan, P. and Moloney, C. (1993). Plastic and other artefacts on South African beaches: temporal trends in abundance and composition. *South African Journal of Science*. 86, pp.450-452.

Ryan, P., Moore, C., van Franeker, J. and Moloney, C. (2009). Monitoring the abundance of plastic debris in the marine environment. *Philosophical Transactions of the Royal Society B: Biological Sciences*, 364(1526), pp.1999-2012.

Small, C. and Nicholls, R.(2003). A global analysis of human settlement in coastal zones. *Journal of Coastal Research* 19(3), pp.584-599.

Somerville, S., Miller, K. and Mair, J. (2003). Assessment of the aesthetic quality of a selection of beaches in the Firth of Forth, Scotland. *Marine Pollution Bulletin*, 46(9), pp.1184-1190.

Song, Y. and Haidvogel, D. (1994). A Semi-implicit Ocean Circulation Model Using a Generalized Topography-Following Coordinate System. *Journal of Computational Physics*, 115(1), pp.228-244.

Thompson, R., Moore, C., vom Saal, F. and Swan, S. (2009). Plastics, the environment and human health: current consensus and future trends. *Philosophical Transactions of the Royal Society B: Biological Sciences*, 364(1526), pp.2153-2166.

Turner, P. and Baptista, A.(1993). ACE/gredit User's Manual. Software for Semi-automatic Generation of Two-Dimensional finite Element Grids. Center for Coastal and Land-Margin Research. Ordegon Graduate Institute of Science & Technology.

Vegter, A., Barletta, M., Beck, C., Borrero, J., Burton, H., Campbell, M., Costa, M., Eriksen, M., Eriksson, C., Estrades, A., Gilardi, K., Hardesty, B., Ivar do Sul, J., Lavers, J., Lazar, B., Lebreton, L., Nichols, W., Ribic, C., Ryan, P., Schuyler, Q., Smith, S., Takada, H., Townsend, K., Wabnitz, C., Wilcox, C., Young, L. and Hamann, M. (2014). Global research priorities to mitigate plastic pollution impacts on marine wildlife.*Endangered Species Research*, 25(3), pp.225-247.

Velander, K. and Mocogni, M. (1999). Beach Litter Sampling Strategies: is there a 'Best' Method?. *Marine Pollution Bulletin*, 38(12), pp.1134-1140.

Yoon, J., Kawano, S. and Igawa, S. (2010). Modeling of marine litter drift and beaching in the Japan Sea. *Marine Pollution Bulletin*, 60(3), pp.448-463.

Zhang, Y., Ateljevich, E., Yu, H., Wu, C. and Yu, J. (2015). A new vertical coordinate system for a 3D unstructured-grid model. *Ocean Modelling*, 85, pp.16-31.

Zhang, Y. and Baptista, A. (2008). SELFE: A semi-implicit Eulerian–Lagrangian finite-element model for cross-scale ocean circulation. *Ocean Modelling*, 21(3-4), pp.71-96.

Zhang, Y., Stanev, E. and Grashorn, S. (2016). Unstructured-grid model for the North Sea and Baltic Sea: Validation against observations. *Ocean Modelling*, 97, pp.91-108.

- Internet resources:

GEBCO (2014) General Bathymetry Chart of the Oceans, British Oceanographic Data Centre, Liverpool, U.K. accessed 10 October 2015,http://www.gebco.net/

Puertos del Estado (2016). Accessed May 1st 2016 <www.puertos.es>